TWO-PHOTON TOTAL INTERNAL REFLECTION MICROSCOPY FOR IMAGING LIVE CELLS WITH HIGH BACKGROUND FLUORESCENCE

A Thesis
Presented to
The Academic Faculty

by

Melinda Anne Ogden

In Partial Fulfillment
of the Requirements for the Degree
Master of Science in the
School of Chemistry and Biochemistry

Georgia Institute of Technology
August 2009

TWO-PHOTON TOTAL INTERNAL REFLECTION MICROSCOPY FOR IMAGING LIVE CELLS WITH HIGH BACKGROUND FLUORESCENCE

Approved by:

Dr. Christine Payne, Advisor
School of Chemistry and Biochemistry
Georgia Institute of Technology

Dr. Rigoberto Hernandez
School of Chemistry and Biochemistry
Georgia Institute of Technology

Dr. Joseph Perry
School of Chemistry and Biochemistry
Georgia Institute of Technology

Date Approved: April 28, 2009

ACKNOWLEDGEMENTS

I would first like to thank Dr. Christine Payne for showing me a line of research which incorporates the interesting components of several very different fields. I always thought the most exciting science is that which combines both the knowledge and questions from different areas. It takes a very talented person with a broad perspective to gather sufficient insight into the most important questions across fields, and then combine and solve them all together. I am very thankful I was able to work with such an individual.

Next I would like to thank all the members of the Payne Lab. With their help and patience, I was able to learn a significant amount of biology content knowledge and microbiology techniques. I do not know too many physical chemists who can say the same. In addition to their knowledge, they offered me their friendship and support which I treasure and appreciate. I only hope I have given as much of myself to them as they have given to me.

I thank Dr. Leigh Bottomley for believing in me as a teacher and for helping me find the right track towards my future.

And finally, though not exclusively, I would like to thank Dr. Joseph Perry and Dr. Rigoberto Hernandez for their support through my degree and their revisions of this document.

TABLE OF CONTENTS

LIST OF FIGURES

LIST OF SYMBOLS AND ABBREVIATIONS

TIR	Total Internal Reflection
GFP	Green Fluorescent Protein
NA	Numerical Aperature
FITC	Fluorescein isothiocyanate
PBS	Phosphate Buffered Saline
Sulfo-SMCC	sulfosuccinimidyl 4-[N-maleimidomethyl]cyclohexane-1-carboxylate
SATA	N-Succinimidyl S-Acetylthiopropionate
EDTA	ethylenediaminetetraacetic acid

SUMMARY

Fluorescence microscopy allows for spatial and temporal resolution of systems which are inherently fluorescent or which can be selectively labeled with fluorescent molecules. Temporal resolution is crucial for imaging real time processes in living samples. A common problem in fluorescence microscopy of biological samples is autofluorescence, fluorescence inherent to the system, which interferes with detection of fluorescence of interest by decreasing the signal to noise ratio.

Two current methods for improved imaging against autofluorescence are two-photon excitation and total internal reflection microscopy. Two-photon excitation occurs when two longer wavelength photons are absorbed quasi-simultaneously by a single fluorophore. For this to take place there must be a photon density on the order of 10^{30} photons/(cm^2)(s), which is achieved through use of a femtosecond pulsed laser and a high magnification microscope objective. Two-photon excitation then only occurs at the focal spot, significantly reducing the focal volume and therefore background autofluorescence.

The second method, total internal reflection, is based on evanescent wave excitation, which decreases exponentially in intensity away from the imaging surface. This allows for excitation of a thin (~200 nm) slice of a sample. Since only a narrow region of interest is excited, an optical slice can be imaged, decreasing excitation of out-of-focus autofluorescence, and increasing the signal to noise ratio.

By coupling total internal reflection with two-photon excitation, an entire cell can be imaged while still maintaining the use of lower energy photons to irradiate the sample and achieve two-photon excitation along the length traveled by the evanescent wave.

This system allows for more sensitive detection of fluorescence of interest from biological systems as a result of a significant decrease in excitation volume and therefore a decrease in autofluorescence signal. In the two-photon total internal reflection microscopy setup detailed in this work, an excitation area of 20 μm by 30 μm is achieved, and used to image FITC-stained actin filaments in BS-C-1 cells.

CHAPTER 1

INTRODUCTION

Biological processes can be probed through a variety of methods. Peptides and proteins can be synthesized or extracted from the host system and combined in a test tube. Information regarding the interactions of these molecules in an ideal, but not realistic environment can then be obtained. This method provides insight into a specific process that may be difficult to probe inside the host system, or to control variables that may be difficult to manipulate otherwise. To truly probe intracellular function, a living intact cell must be used. Working with living cells provides insight into dynamic events, and allows the investigation to take place in the native environment.

Probing the dynamics of living cells without disrupting the function of interest is crucial. This constraint is overcome through a technique called fluorescence microscopy. In fluorescence microscopy, the cellular component of interest is tagged, and this fluorescent tag is monitored with a microscope and a powerful camera. Fluorescence is a process in which a molecule, called a fluorophore, is brought from its ground electronic state to its excited electronic state by absorption of a photon [1]. Once this fluorophore has reached the excited state, it relaxes back to the ground state through emission of a photon which is slightly lower in energy than the photon which was initially absorbed. The emitted photons from the tag are then monitored with a camera, and the actions of the cellular component of interest can be deduced. Introduction of multiple tags allows for investigations of intracellular interactions between multiple components [2].

The fluorophore tags used in live cell imaging can be small organic molecules such as fluorescein or rhodamine, or they can be fluorescent proteins. Fluorescent proteins can be introduced to the cell through a process called transfection [3]. During transfection, DNA which codes for production of the fluorescent protein is introduced to

the cell, and once the cell has incorporated this DNA into its own genetic code, the fluorescent protein is produced by the cell each time the cellular DNA is translated. To tag a specific protein which is involved in a function of interest within a cell, the DNA for the fluorescent protein is introduced into the cellular DNA in a location adjacent to the DNA segment which codes for protein of interest. Now each time the protein of interest is expressed, the fluorescent protein will also be expressed.

Several hurdles exist for imaging live cells with fluorescence microscopy. The main concerns are to keep the cells alive and healthy, and to obtain the highest quality images possible. The high photon flux necessary for fluorescence microscopy can be damaging to both the cell and the fluorophores. Damage to the cell due to photon flux is termed photodamage. Fluorophores damaged by photon flux enter a dark state in which they are no longer fluorescent [4]. This loss of fluorophore emission after many cycles of fluorescence excitation and emission is called photobleaching. Photobleaching and photodamage result in decreased cell health and image quality, and must be carefully monitored and reduced during fluorescence microscopy imaging.

There are many different configurations of fluorescence microscopy systems [5]. The most widely used are discussed below with comparisons drawn between them.

Current Fluorescence Microscopy Methods

The most commonly used fluorescence microscopy method is the standard widefield method (Figure 1.1A) in which a large area of several hundred square microns is illuminated at one time [5]. This method allows for imaging of several cells at a rate limited by CCD camera acquisition, typically greater than 35 frames per second. However, the incident excitation light penetrates through the entire z-dimension of the cells, resulting in noticeable photobleaching and photodamage for prolonged experiments. With this extensive z excitation, out-of-plane fluorescence signal can decrease the quality of the resulting images.

To help overcome the problem of out-of-focus signal, confocal microscopy was developed [6]. In this configuration (Figure 1.1B), a pinhole is introduced between the sample and the detector. The pinhole rejects out of focus fluorescence signal, resulting in an increase in signal to noise. The entire sample is still subject to the incident excitation, so the level of photobleaching and photodamage would be similar to that for a widefield setup. Although the pinhole increases the quality of the images, it introduces a new disadvantage: the need for scanning of the excitation source across the sample to produce an entire image. Scanning is usually carried out by two galvanometrically driven mirrors which move synchronously to scan the excitation source across the sample. With this new requirement, some temporal information is lost, since the imaging is now limited by the scanning rate, typically 5 frames per second.

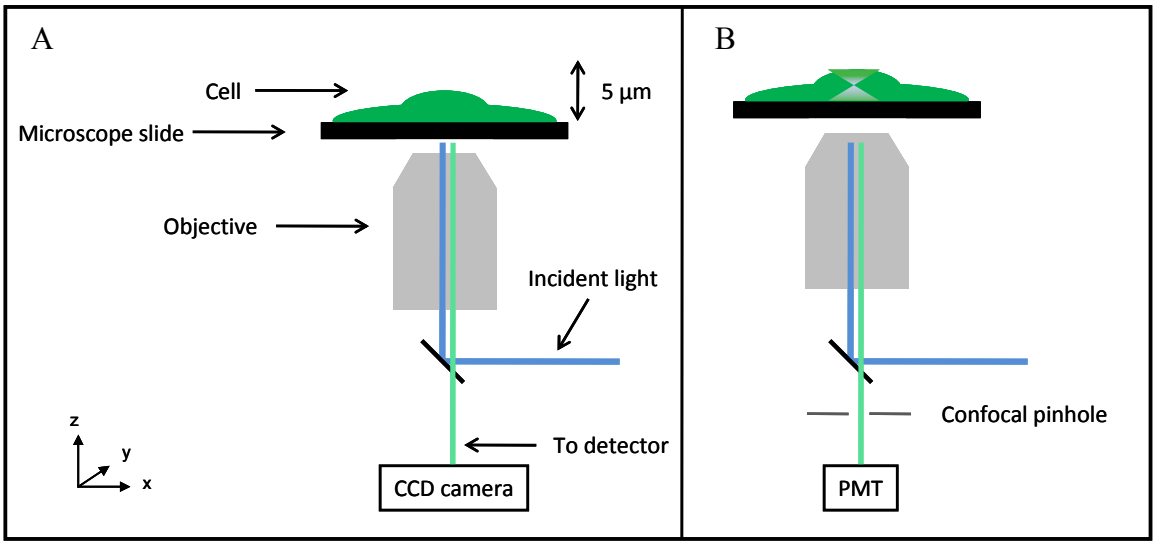

Figure 1.1. Schematic of widefield (A) and confocal (B) microscopy systems.

Two-photon excitation microscopy combines the advantages of confocal microscopy with the improvement of limited photobleaching and photodamage. In comparison with the standard one-photon methods described above in which one photon excites the fluorophore from the ground to excited state, in two-photon excitation, two photons must be absorbed by the fluorophore within 5 femtoseconds of each other in order for excitation to occur (Figure 1.2A) [7]. The absorption of two photons imposes

the requirement of a high photon density, on the order of 10^{30} photons/(cm^2)(s) [7]. This photon density is achieved through the use of a pulsed femtosecond laser to cluster the photons in time and a microscope objective to focus the light spatially. Due to the density requirement, excitation is only achieved at the focal spot, which essentially eliminates out of focus excitation and reduces photobleaching and photodamage throughout the sample (Figure 1.2B). However, as with confocal microscopy, the excitation source must be scanned across the sample to produce an entire image, limiting the temporal resolution to the scanning rate of 5 frames per second.

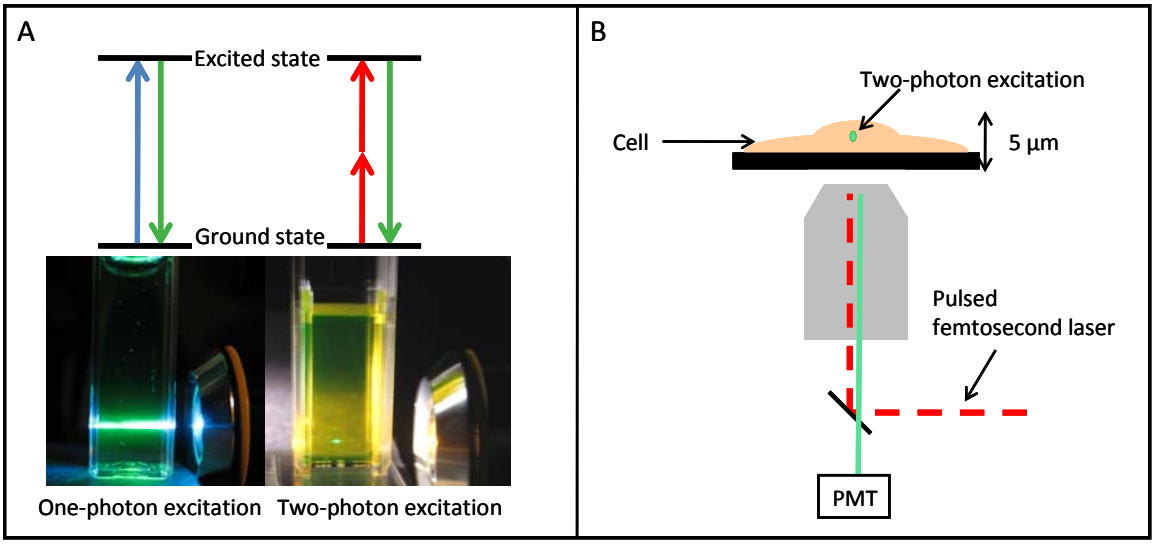

Figure 1.2. A. One and two-photon excitation of fluorescein in a cuvette. Wavelengths of excitation are 458 nm and 800 nm, respectively. B. Schematic of two-photon excitation microscopy method.

Since in the two-photon method the excitation source has long wavelength photons, and cellular autofluorescence (fluorescence endogenous to the system) occurs in the blue region of the spectrum [8], virtually no autofluorescence occurs. This is illustrated in Figure 1.3, which shows one and two-photon excitation of BS-C-1 (green monkey kidney [9]) cells with only endogenous fluorophores present.

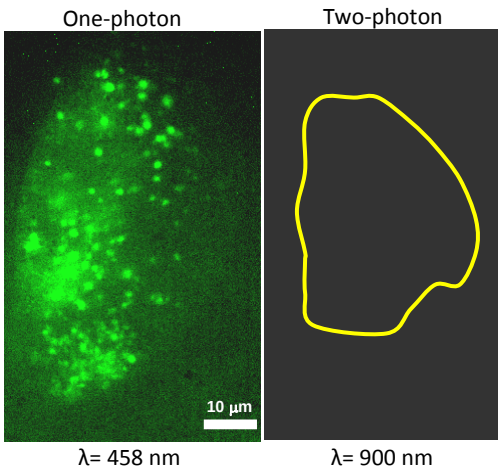

Figure 1.3. One and two-photon excitation of cellular autofluorescence. Cell location is outlined in yellow on two-photon image.

Another microscopy method which has minimal excitation of out of focus fluorophores, and maintains the temporal resolution present in the widefield configuration, is total internal reflection (TIR) microscopy. This method is configured similarly to the widefield method, but the excitation light is brought in off-axis in the back of the objective, which forces the light to exit the objective at an angle [10]. When the light is at the correct angle, given by Snell's Law:

$$\theta_{crit} = \sin^{-1}\left(\frac{n_2}{n_1}\right)$$

and is incident on an interface of two media with different indices of refraction, total internal reflection of the incident light occurs [9]. A small, imaginary component of the incident light propagates along the surface at the interface, and decays exponentially in the z direction. This component is called the evanescent wave, and results in an excitation depth of approximately 200 nm (Figure 1.4). This small excitation depth provides the method with good signal to noise capabilities as with confocal and two-photon microscopies, but with the improvement of having an imaging area comparable to that of the widefield method.

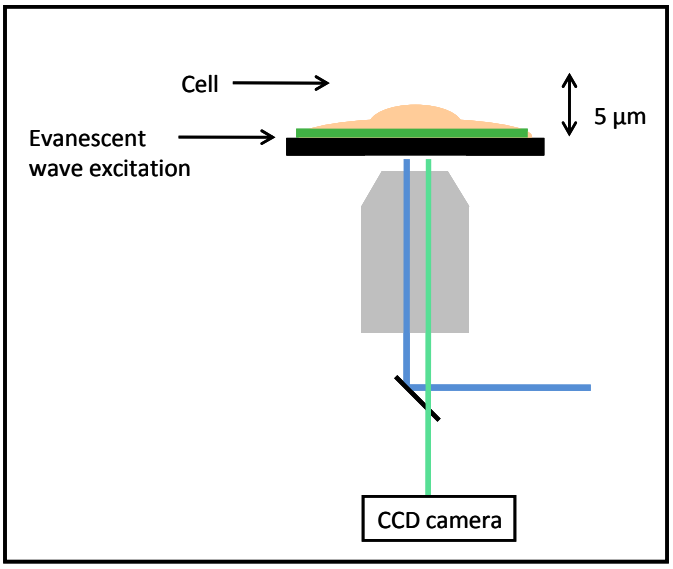

Figure 1.4. Schematic of total internal reflection microscopy.

The excellent signal to background advantage of TIR is shown in Figure 1.5. The signal to background in the widefield configuration is 1.3, as compared with a signal to background of 6 in TIR. These are images of 200 nm fluorescent polystyrene beads, some of which are in solution, and some of which have fallen onto the glass coverslip. In the TIR configuration, only the beads which have fallen on the coverslip are within the area of excitation provided by the evanescent wave, so the out of focus beads are not excited and therefore do not contribute to any background signal. In both widefield and TIR, the excitation wavelength is 488 nm.

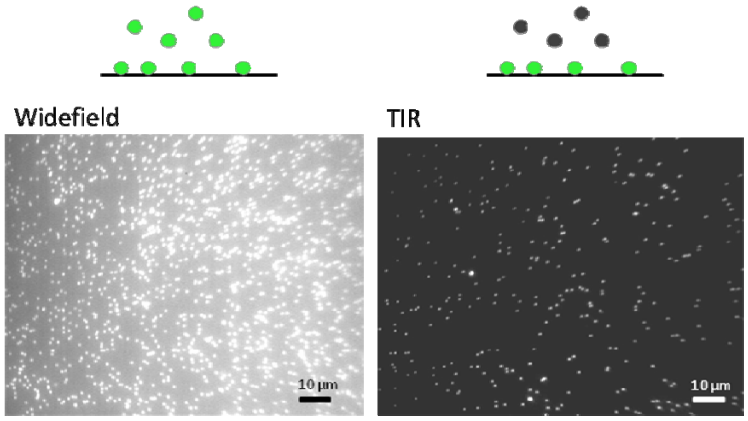

Figure 1.5. Excitation of 200 nm fluorescent polystyrene beads in the widefield and TIR configurations.

Total internal reflection microscopy combines the advantages of widefield and confocal microscopies, but with low-wavelength photons that are capable of exciting cellular autofluorescence. Two-photon excitation has good signal-to-noise as with the confocal method, and no excitation of autofluorescence, but still suffers from decreased temporal resolution due to the need for scanning. Most systems can be studied using one of these four methods, but the two systems described below need minimal excitation of out-of-focus fluorophores, high temporal resolution, and the use of long-wavelength photons.

Systems which would benefit from an improved imaging system.

Huntington's disease is a hereditary neurodegenerative disease affecting 5 in 100,000 people in the United States [11]. As with other neurodegenerative diseases, like Alzheimer's disease, there is no cure and little understanding of the causes of symptoms. A characteristic of Huntington's disease is the formation of aggregates of the mutant Huntingtin protein [12]. At this time, the method of aggregate formation and the role of the aggregates in cell death are unknown.

A model system for studying aggregation related to Huntington's disease is a PC12 cell line which has the mutant Huntingtin protein labeled with green fluorescent protein (GFP). Aggregation of the mutant protein can be imaged in these cells as punctate areas of increased GFP intensity. Since the mutant protein is present throughout the cell, there is a diffuse signal from the GFP in the entire cytosol. This makes imaging the aggregates challenging, since there is a very high background signal resulting from precisely the protein of interest (Figure 1.6).

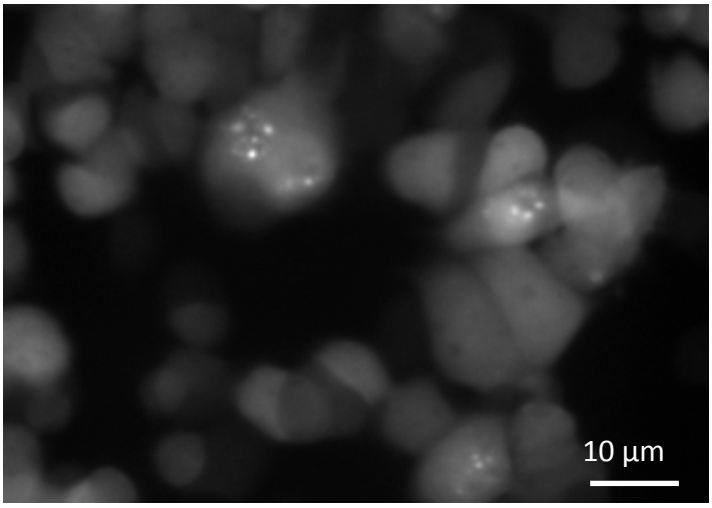

Figure 1.6. Aggregation of mutant Huntingtin protein labeled with GFP in PC12 cells.

Although aggregates can be seen in Figure 1.6, their formation at the early stages is difficult to monitor against the high background. Without the capability to probe early aggregate formation, the cause of aggregation can not be determined. An imaging system which employs long wavelength photons but maintains high temporal resolution is needed for investigation of early aggregate formation in this model system for Huntington's disease.

A second system which is difficult to image with current methods is bacteria. Bacteria are known to be highly autofluorescent [13], which makes imaging of non-endogenous fluorophores extremely difficult. Figure 1.7a shows endogenous fluorescence from *E. coli* imaged in a one-photon widefield configuration with 488nm excitation. It is clear that additional non-endogenous fluorophores would be lost within this high background signal. The use of two-photon excitation (Figure 1.7b, 800nm excitation) or TIR would help to resolve this issue, as minimal excitation of background endogenous fluorophores would occur. A combination of two-photon and total internal reflection microscopies would allow for improved imaging of these two systems, as well as others currently being studied with the methods described previously.

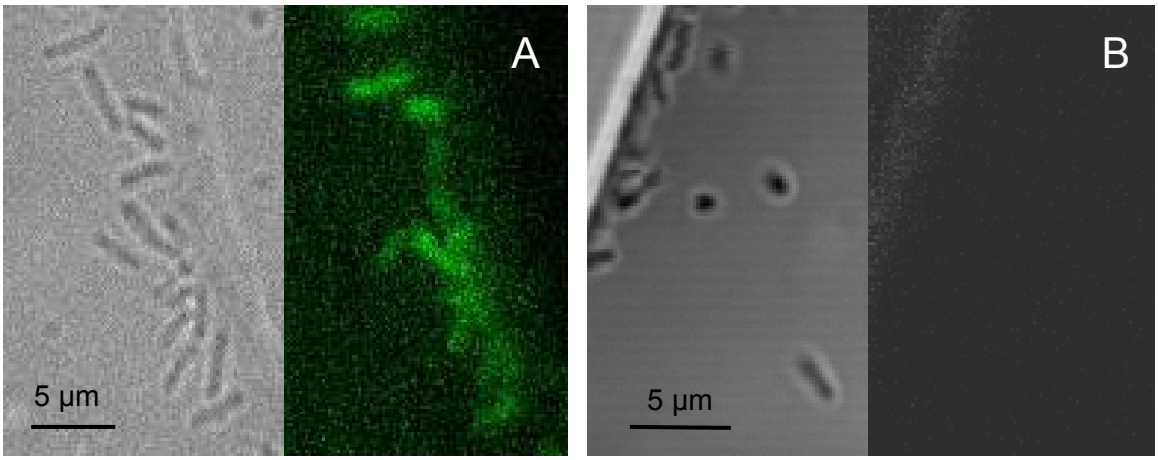

Figure 1.7. Excitation of endogenous fluorophores in *E. coli* in a one-photon widefield configuration with 488 nm excitation (A) and a two-photon scanning configuration with 800 nm excitation (B).

CHAPTER 2

TWO-PHOTON TOTAL INTERNAL REFLECTION MICROSCOPY

Two-photon total internal reflection microscopy, developed by Oheim in 2003 [14], combines the advantages of two-photon microscopy with total internal reflection. This combination allows for the use of low energy photons but with a large excitation area on the order of 500 square microns. Imaging of large areas of single cells with high background fluorescence becomes possible with this novel method.

Two-photon excitation.

Two-photon excitation, proposed in 1931 by Maria Göppert-Mayer [15], was achieved experimentally in 1961 after the invention of the laser [16]. Two-photon microscopy was developed in 1990 by Denk, Strickler and Webb [17]. Two-photon excitation occurs as a result of quasi-simultaneous absorption of two photons to excite a molecule from the ground to excited state. This absorption process occurs through a virtual state that has a lifetime of 5 femtoseconds [7]. It is then within this time scale that the two photons must be absorbed. The presence of the virtual state results in a selection rule for two-photon absorption different than that for one-photon absorption. Instead of the ground and excited states being of different symmetry, as in the one photon case, they must be of the same symmetry (Figure 2.1). This is because the virtual state will be of the opposite symmetry of the ground and excited states, so the general selection rule still holds. The derivation of this selection rule follows.

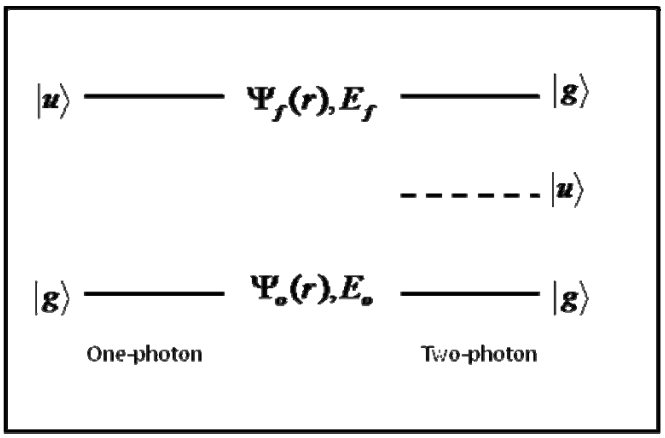

Figure 2.1. Energy levels and symmetry in a one-photon and two-photon system.

The excitation from the ground to excited state requires an energy ħω:

$$E_f = E_o + \hbar\omega_k \tag{1}$$

This event has a probability, $\omega_{f\leftarrow o}$ given by

$$\omega_{f\leftarrow 0}^{(n)} = \left(\frac{2\pi}{\hbar}\right)\left|\langle f|M|0\rangle\right|^2 \rho^n(E)d^{n-1}E \tag{2}$$

where M is the n[th] order matrix element and $\rho^n(E)d^{n-1}E$ is the density of initial photon states, $\rho(E)$. For the probability to be non-zero, the transition matrix element of the interaction of the Hamiltonian between the two states must be non-zero:

$$\langle \psi_f; n_{k-1}|H'|n_k; \psi_o\rangle \neq 0 \tag{3}$$

where n is the number of photons and H' is the interaction Hamiltonian for the interaction of electromagnetic radiation with the electrons in the molecule.

$$H' = \sum_{j=1}^{N} -\left(\frac{e_j}{m_j c}\right)p_j \bullet A_j + \left(\frac{e_j^2}{2m_j c^2}\right)A_j \bullet A_j \tag{4}$$

Here p_j is the momentum vector of the j[th] electron, and A_j is the vector potential for the light wave at position r_j, and is given by:

$$A_j = \sum_{k,\sigma} A_{k\sigma}\left[\frac{2\pi\hbar c^2}{\omega_k V}\right]^{1/2} e_{k\sigma}\left[a_{k\sigma}\exp\left(i\vec{k}\cdot r\right) + a_{k\sigma}^{+}\exp\left(-\vec{k}\cdot r\right)\right] \tag{5}$$

where $e_{k\sigma}$ is the polarization vector. Now an event has been isolated in which the number of photons in the k[th] mode has decreased by one and the molecule has changed its electronic distribution from ψ_o to ψ_f.

The overall matrix element from one-photon absorption is then:

$$\left\langle \psi_f ; n_{k\sigma-1} \left| H^{'} \right| n_{k\sigma} ; \psi_o \right\rangle = -\sqrt{n_{k,\sigma}} \sum \frac{e_j}{m_j} \sqrt{2\pi\hbar / w_k V} \int \psi_f^* \left(p_j \cdot e_k \right) \exp\left(i\vec{k} \cdot r_j \right) \psi_o d\tau \qquad (6)$$

And the transition probability for a one-photon absorption is:

$$w_{f \leftarrow o} = \frac{4\pi^2}{\hbar\omega_k} \frac{n_{kp}(E_k)}{V} \left(\frac{e^2}{m^2} \right) \left\{ \int \psi_f^* p e_k \exp\left(i\vec{k} \cdot r \right) \psi_o d\tau \right\}^2 \qquad (7)$$

where $\frac{n_{kp}(E_k)}{V}$ is the number of photons per unit volume. The exponential term can be set equal to one because of the dipole approximation. This then gives

$$\omega \propto \int \psi_f^* r \psi_o d\tau . \qquad (8)$$

If both wavefunctions are even functions of *r,* then the integrand is odd, and the integral vanishes. Therefore, since the ground state is even (gerade), the excited state for a one-photon process must be odd (ungerade) to have a non-vanishing integral. In the two-photon case, excitation from the gerade ground state to a gerade excited state passes through the ungerade virtual state, maintaining the above derived selection rule.

In order for two photons to be absorbed by the molecule within the lifetime of the virtual state, a photon density on the order of 10^{30} photons/(cm^2)(s) is required [7]. This photon density is achieved through use of a femtosecond laser and a spatial focusing of the beam through use of a microscope objective.

The femtosecond laser produces pulses of light on the order of 100 fs in length at a repetition rate of 80MHz as a result of Kerr lens modelocking in a non-linear titanium-doped sapphire crystal [18]. When intense light propagates through a non-linear crystal, a change in refractive index of the crystal occurs, the extent of which is dependent on the

intensity of the light and in a resonator cavity results in a focusing of the beam. With the introduction of a noise spike, and subsequent amplification of the spike as it travels around the cavity, a pulse of light is produced. The remaining continuous wave light which is not pulsed does not produce a change in the index of refraction of the crystal, and so is not focused. The difference in beam width of the pulsed and continuous wave light allows for rejection of the continuous wave light with a hard aperature at the end of the cavity. The combination of the Kerr effect with an optimally designed cavity therefore results in the production of high photon density laser pulses used for two-photon excitation.

The excitation volume resulting from the spatial focusing and use of femtosecond pulses is on the order of a femtoliter, which necessitates the use of scanning for production of an entire microscopy image. To effectively spread this excitation volume in the lateral dimensions, total internal reflection is employed.

Total internal reflection

Total internal reflection fluorescence microscopy, developed by Axelrod [10], is used throughout the life sciences for improved imaging over confocal microscopy. Total internal reflection occurs when light incident on an interface between two media of different refractive indices is brought in at an angle called the critical angle. The critical angle is a function of the refractive indices and is given by

$$\theta_{crit} = \sin^{-1}\left(\frac{n_2}{n_1}\right) \tag{9}$$

Where n_2 and n_1 are the refractive indices of the two media. The imaginary component of the wave vector, called the evanescent wave, will propagate along the surface at the interface with an intensity decaying exponentially in the z direction. It is with this evanescent wave that fluorescence microscopy can be performed, using the 200 nm

effective penetration depth of the wave. The derivation of the evanescent wave from Maxwell's equations follows.

First, an expression for transverse plane waves must be derived. Starting with Maxwell's equations in a vacuum:

$$\begin{aligned} \nabla \bullet E &= 0 & \nabla \times E + \frac{\partial B}{\partial t} &= 0 \\ \nabla \bullet B &= 0 & \nabla \times B - \mu\varepsilon \frac{\partial E}{\partial t} &= 0 \end{aligned} \tag{10}$$

Decoupling the partial differential equations for E and B by application of the curl:

$$\begin{aligned} \nabla \times (\nabla \times E) &= \nabla(\nabla \bullet E) - \nabla^2 E \\ \nabla \times (\nabla \times B) &= \nabla(\nabla \bullet B) - \nabla^2 B \end{aligned} \tag{11}$$

Substituting:

$$\begin{aligned} \nabla \times \left(\frac{-\partial B}{\partial t} \right) &= \frac{-\partial}{\partial t}(\nabla \times B) = -\mu\varepsilon \frac{\partial^2 E}{\partial t^2} \\ \nabla \times \left(\mu\varepsilon \frac{\partial E}{\partial t} \right) &= \mu\varepsilon \frac{\partial}{\partial t}(\nabla \times E) = -\mu\varepsilon \frac{\partial^2 B}{\partial t^2} \end{aligned} \tag{12}$$

Using the first two Maxwell equations, E and B are completely decoupled:

$$\begin{aligned} \nabla^2 E &= \mu\varepsilon \frac{\partial^2 E}{\partial t^2} \\ \nabla^2 B &= \mu\varepsilon \frac{\partial^2 B}{\partial t^2} \end{aligned} \tag{13}$$

Now each Cartesian component of the electric and magnetic fields satisfies

$$\nabla^2 u - \frac{1}{v^2} \frac{\partial^2 u}{\partial t^2} = 0 \text{ with } v = \frac{c}{\sqrt{\mu\varepsilon}} \tag{14}$$

For a plane wave the fields are uniform over every plane perpendicular to the direction of travel. The solution is then

$$\begin{aligned} u &= \exp\left(i\vec{k} \cdot \vec{x} - i\omega t\right) \\ k &= \frac{\omega}{v} = \sqrt{\mu\varepsilon}\, \frac{\omega}{c} \end{aligned} \tag{15}$$

With the wave propagating in only one direction, the fundamental solution is

$$u(x,t) = A\exp(ikx - i\omega t) + B\exp(-ikx - i\omega t) \tag{16}$$

In the medium with lower refractive index, this solution can be written as (18):

$$\vec{E}_1 = \vec{E}_{10}\exp[i(\vec{k}_1\vec{x} - \omega t)] = \vec{E}_{10}\exp[i(\vec{k}_{1x}\vec{x} + \vec{k}_{1z}\vec{z} - \omega t)] = \vec{E}_{10}\exp[i(\vec{k}_1\sin\theta\cdot\vec{x} + \vec{k}_1\cos\theta\cdot\vec{z} - \omega t)]$$

Since

$$\begin{aligned}\vec{k}\cdot\vec{r} &= \vec{k}(\sin\theta_t, \cos\theta_t, 0)\cdot(x,y,z),\\ \vec{k}\cdot\vec{r} &= \vec{k}(x\sin\theta_t + y\cos\theta_t)\end{aligned} \tag{18}$$

Then

$$\cos\theta_t \equiv \sqrt{1-\sin^2\theta_t} = \sqrt{1-\frac{\sin^2\theta}{n_{12}}} \tag{19}$$

where n_{12} is the ratio of refractive indices at the interface. At the critical angle, $\sin\theta = n$ and $\cos\theta = 0$. For angles where $\sin\theta > n$, TIR occurs and $\cos\theta$ becomes imaginary:

$$\cos\theta_t = i\sqrt{\frac{\sin^2\theta}{n_{12}} - 1} \tag{20}$$

Combining this expression for $\cos\theta$ (20)with the solution for the electromagnetic wave in the lower indexed medium (18), the final solution is obtained:

$$\vec{E}_1 = \vec{E}_{10}\exp[i(\vec{k}n_{12}^{-2}\sin\theta_t\cdot\vec{x} - \omega t)]\times\exp\left(-\vec{k}_1\sqrt{n_{12}^{-2}\sin^2\theta_t - 1}\cdot\vec{z}\right) \tag{21}$$

The first part of this equation describes the propagation of the wave in the forward direction, and the second part shows the exponential decay in the z direction.

The combination of two-photon excitation with total internal reflection allows for the use of low energy photons with an expanded imaging area. The next chapter will outline how two-photon total internal reflection is achieved experimentally, and demonstrate its use in imaging fluorescent molecules or proteins in cells.

CHAPTER 3

FLUORESCENCE IMAGING WITH TWO-PHOTON TOTAL INTERNAL REFLECTION MICROSCOPY

Experimental Setup

A modelocked titanium:sapphire laser (Coherent) tuned to a wavelength of 750 nm with a 80MHz repetition rate was expanded to fill the back of a 60x 1.4 NA oil immersion objective (Olympus). An inverted microscope (Olympus IX-70) was used in an epifluorescence configuration with a 620 nm short pass dichroic mirror and a 510-560 nm bandpass emission filter (Chroma). Fluorescence emission was imaged on an electron-multiplying CCD camera (Andor Ixon- DU888), and data was collected using the imaging software Micro-Manager. In this configuration, the presence of two photon excitation of a 10 μM sodium fluorescein solution in water was verified. A one micron by one micron area of fluorescein solution showed emission when excited at 750 nm. When modelocked, the laser produces ultrashort pulses as a result of a fixed phase relationship between the modes of the resonator cavity. In the absence of modelock, pulses are not produced, and only continuous wave light is present, which does not condense the photons in time. In this situation (no modelock), all sample emission was absent. A power study was also done to ensure two-photon excitation was responsible for the emission from the fluorescein (Figure 3.1).

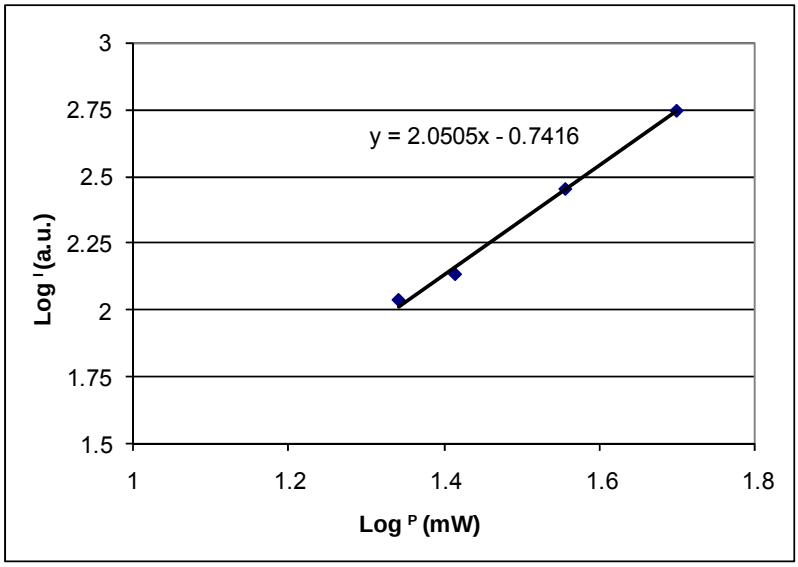

Figure 3.1. Two-photon intensity dependence. *I* is fluorescence intensity, and *P* is incident laser power.

In order to achieve total internal reflection, the laser beam was expanded and collimated before being focused onto the back focal plane of the microscope objective. The beam expander was comprised of a -100 mm focal length expanding lens and a 200 mm focal length collimating lens. The focusing lens had a focal length of 400 mm and was placed seven inches from the back of the microscope. This configuration resulted in a collimated beam exiting the objective, providing an excitation area of 16 μm by 20 μm. Once two-photon excitation of fluorescein was confirmed as above, total internal reflection was attempted. In order for the beam to be incident off-axis on the back of the objective, the focusing lens and final turning mirror before the microscope were mounted on a translation stage (Figure 3.2). When the stage was translated 10 mm, total internal reflection was achieved, providing an excitation area of 20 μm by 30 μm.

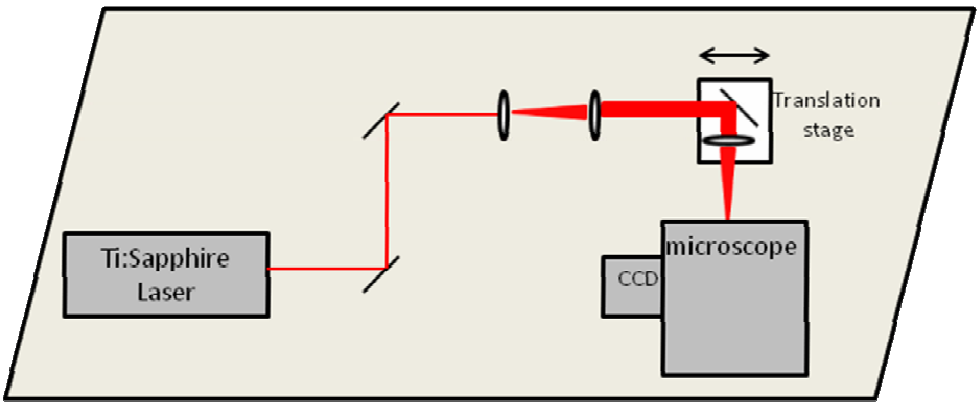

Figure 3.2 Two-photon total internal reflection microscopy setup.

Results

TIR was confirmed by imaging 200 nm 500/515 fluorescent polystyrene beads (Invitrogen). In standard epifluorescence, both beads which had fallen onto the surface of the coverslip and beads still in solution were visible (Figure 3.3a). Slow translation of the stage to convert from epifluorescence to total internal reflection resulted in an increase of the signal to noise in images of the beads (Figure 3.3b). After passing the critical angle, all emission disappeared as a result of the loss of the evanescent wave. Translation back to the point at which excitation of the beads was achieved was deemed the critical angle, and therefore excitation by two-photon total internal reflection. Two-photon excitation was confirmed with a power study as in Figure 3.1, as well as an absence of fluorescence in the absence of modelocking. In this two-photon TIR configuration, only the beads which had fallen onto the coverslip were visible, as confirmed by a greater signal-to-background than in the epifluorescence configuration.

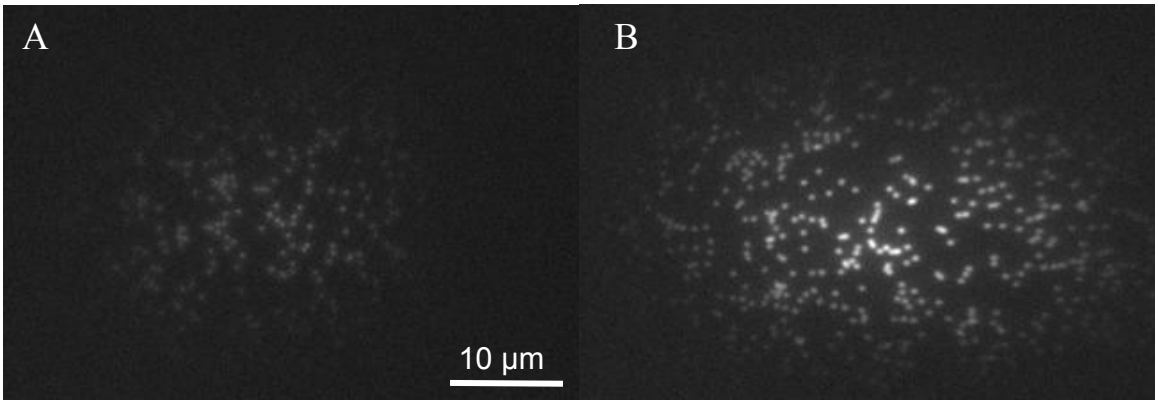

Figure 3.3. Two-photon excitation of 200 nm fluorescent polystyrene beads in standard epifluorescence (A) and total internal reflection (B). Signal to background for epifluorescence is 3.3, and for TIR is 11.7.

Fluorescein isothiocyanate (FITC)-stained actin in BS-C-1 cells was also imaged. Images were taken with a 700 ms exposure time in the two-photon configuration (Figure 3.5) and 100 ms exposure time in the one-photon configuration (Figure 3.4) using a Hg/Xe lamp for excitation.

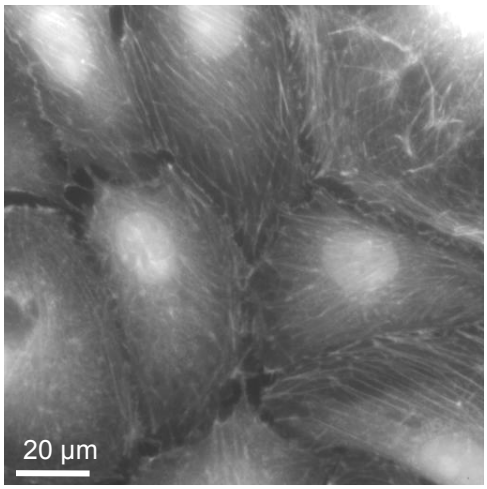

Figure 3.4. One-photon excitation of FITC-stained actin filaments in BS-C-1 cells.

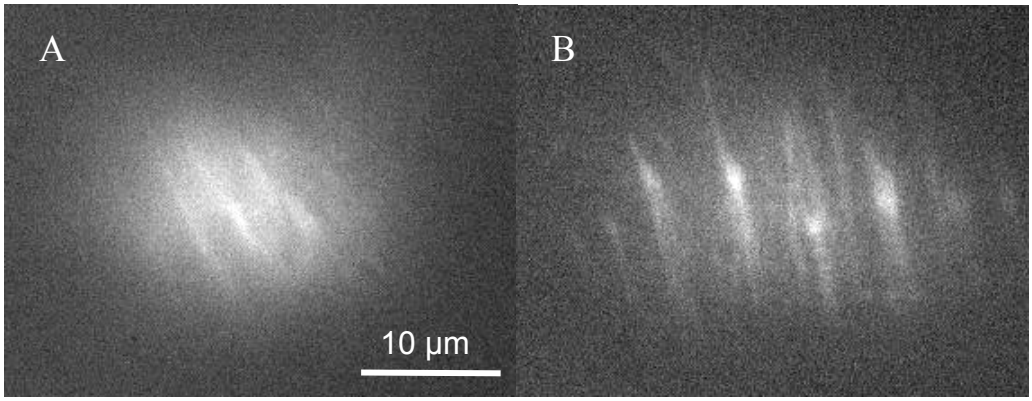

Figure 3.5. Two-photon excitation of FITC-stained actin filaments in BS-C-1 cells. A. standard epifluorescence configuration. B. TIR configuration.

Photobleaching characterization was performed for comparison between one- and two-photon excitation. Characterization was performed on FITC-stained actin in BS-C-1 cells (see above). The one-photon excitation source was an argon-ion laser (Melles Griot) at 488nm and 36.5 mW. CCD exposure time was 300 ms. The two-photon excitation source was a femtosecond Ti:Sapphire laser (Coherent) at 750 nm and 34 mW at the sample. Exposure time was 700 ms. As seen in Figure 3.6, photobleaching in the two-photon TIR configuration is comparable to that for the one-photon epifluorescence configuration.

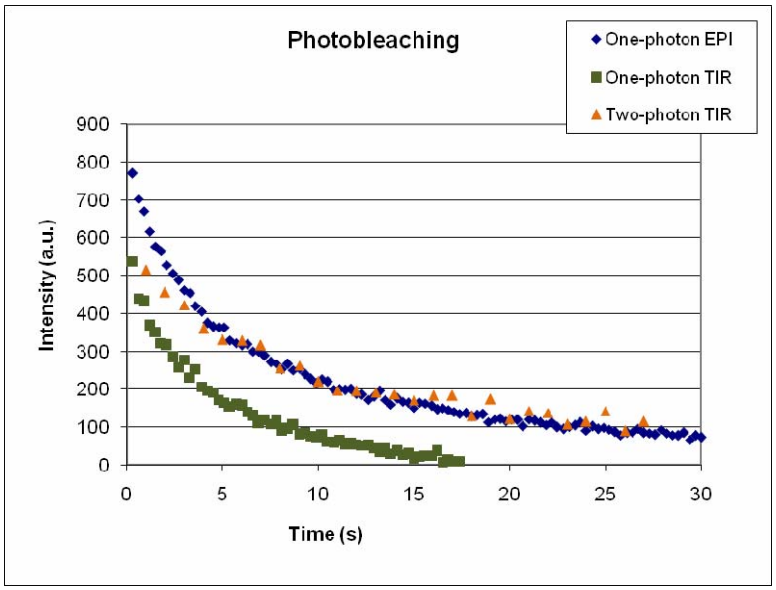

Figure 3.6. Photobleaching of FITC-stained actin filaments in BS-C-1 cells for one- and two-photon excitation. No increase is photobleaching is seen for the two-photon excitation.

Conclusion

In conclusion, two-photon total internal reflection microscopy provides a method for imaging cells using low energy photons in real time. With a significant increase in signal to background with comparison to the standard epifluorescence two-photon configuration, and without an increase in photobleaching, two-photon TIR will prove essential for imaging biological systems with inherently high background signal.

In this work, it was shown that a two-photon excitation area of 20 μm by 30 μm was achieved through use of a two-photon total internal reflection microscopy configuration. Using this large excitation area, a significant portion of fluorescently-stained mammalian epithelial cells could be imaged with low-energy photons and a time resolution limited only by CCD acquisition rate. An almost 4-fold increase in signal to background was achieved for two-photon TIR as compared with two-photon widefield excitation using the same lens configuration. Fluorescence imaging studies on systems with inherently high background signal will benefit from this microscopy system.

APPENDIX A

LASER ALIGNMENT AND TIR

The alignment of the Coherent MIRA laser cavity is described in the Operator's Manual in detail. Following are additional guidelines for successful MIRA cavity alignment.

In practice, the wavelength at which the MIRA is most stable is 750 nm. At this wavelength and 5 W of pump power from the Coherent VERDI, average output power is 550 mW. This power results in approximately 300 mW delivered to the sample using a 60x objective and the beam path outlined in Figure 3.2. In this configuration, the power at the focus scales linearly with average laser output power by the relation given in Figure A.1.

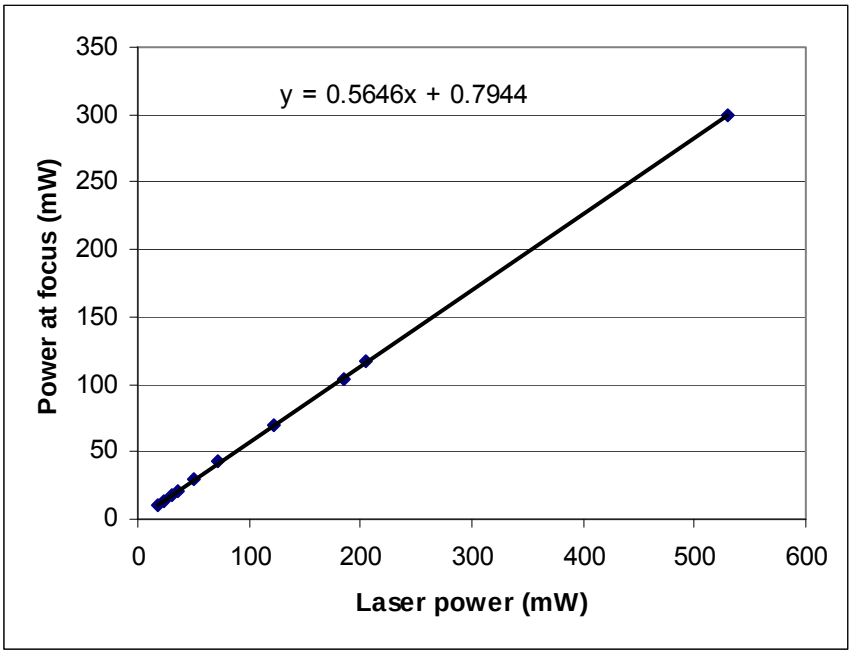

Figure A.1. Relationship between average laser output power and power delivered to sample using 60x objective and configuration in Figure 3.2.

During alignment, it is not advisable to adjust the mirror or lens right before the crystal (lens L1, mirror M4), as this could result in the beam being incident on the crystal in an off-axis configuration which will damage the crystal.

If modelock is not achieved, it is advisable to tune the wavelength to 750 nm or 800 nm. At 750 nm, the prism positions should be near 10.2 for BP1 and 10 for BP2. At 800 nm the prism positions should be 10.25 for BP1 and 6 for BP2. Introduction of more prism glass into the beam path will result in shorter pulses, but a more difficult time modelocking. An IR viewer must be used to visualize the beam passing through BP2. Pulse length can be monitored with an oscilloscope. If modelock is not achieved in one of these configurations, realignment of the cavity may be necessary. Follow the instructions in the user's manual, but without adjusting mirror M4 or lens L1. If a strong weather front is moving through, it may be the cause for an absence of modelock, and waiting until it passes may be more advisable than cavity realignment.

Once the laser is modelocked and the beam is aligned into the microscope, the presence of two-photon excitation should be checked using 200 nm polystyrene 500/515 fluorescent beads in a PBS solution (or other wavelength-appropriate fluorescent beads). If no signal from the beads is observed either through the eyepiece or on the camera, check for modelocking. If modelock is lost, see if it can be regained by blocking the beam before it enters the microscope. If this is the case, then when the beam enters the microscope and is incident on the sample, a back reflection is traveling back down the beam path and into the MIRA cavity, causing a loss of modelock. In this case, a slight misalignment of the collimating lens will solve the problem.

After two-photon excitation of fluorescent polystyrene beads is confirmed, translation into TIR can be checked with the beads. Translation of the translation stage behind the microscope from a position of 2 to 4 should result in TIR. During translation of the stage, the beam will exit the microscope objective at an angle. Extreme caution should be taken when translating the beam, and the beam block built for the microscope

should be employed. Once the beam has disappeared from the wall or the beam block, TIR has been achieved, and should be confirmed with an increase in signal to background of the fluorescent beads as compared with the standard epifluorescence configuration. In the event that TIR is not achieved, realignment of the beam from the cavity to the microscope should be performed.

APPENDIX B

PROTOCOLS FOR CELL PREPARATIONS

BS-C-1 cells were grown to 80% confluency before staining actin with FITC-phalloidin. Before staining, cells were fixed with formaldehyde. Cells were washed twice with phosphate buffered saline (PBS). 1 mL of 3.7% formaldehyde in PBS was added to the cells, and incubated at room temperature for 10 minutes. Cells were then washed five times with PBS. 1 mL of 0.1% Triton X-100 in PBS was added, and the cells were incubated at room temperature for five minutes, and subsequently washed five times with PBS. 500 μL of 0.025 mg/mL FITC-phalloidin (Sigma) in 25% methanol/ 75% PBS solution were added to the cells, which were then rocked at room temperature for 20 minutes. Cells were washed five times before imaging.

Expression of the Huntingin-GFP fusion protein was induced by activation of the Tet-on promoter in the presence of 1μg/mL Dox [19].

APPENDIX C

SURFACE FUNCTIONALIZATION OF FLUORESCENT NANOMETER-SCALE POLYSTYRENE BEADS

A separate project involving the surface functionalization of fluorescent polystyrene beads was performed. The ultimate goal of this functionalization was for delivery of the beads to the cytosol of living cells as fluorescent probes. The delivery mechanism requires the bead to have streptavidin present on the surface for conjugation to biotin-modified polyarginine. The method of delivery has been used for delivery of quantum dots [20], however the mechanism of bead uptake by the cells is not fully understood. By modifying the polystyrene beads, a size dependence of the mechanism can be probed, since the beads are available in a wide range of sizes.

Modification of surface amine groups on 40 nm polystyrene beads was performed. The beads are fluorescent with an absorption peak at 520 nm and an emission peak at 580 nm. Functionalization with streptavidin was achieved through a maleimide/thiol linker.

First, the amine-coated beads were modified with sulfo-SMCC to provide a maleimide surface. Second, free streptavidin was modified with SATA to provide a free thiol group on the protein.

Sulfo-SMCC

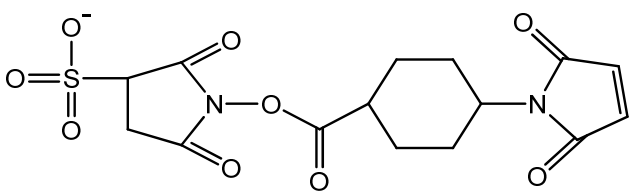

SATA

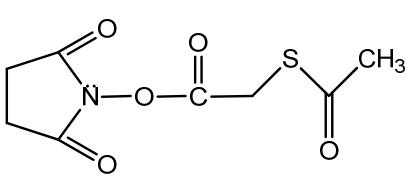

Figure C.1. Structure of sulfo-SMCC and SATA.

Reaction of the maleimide-coated beads and the thiolated streptavidin resulted in conjugation giving streptavidin-coated beads. The biotin-binding capability of the streptavidin on the beads was tested.

A reaction scheme is given below:

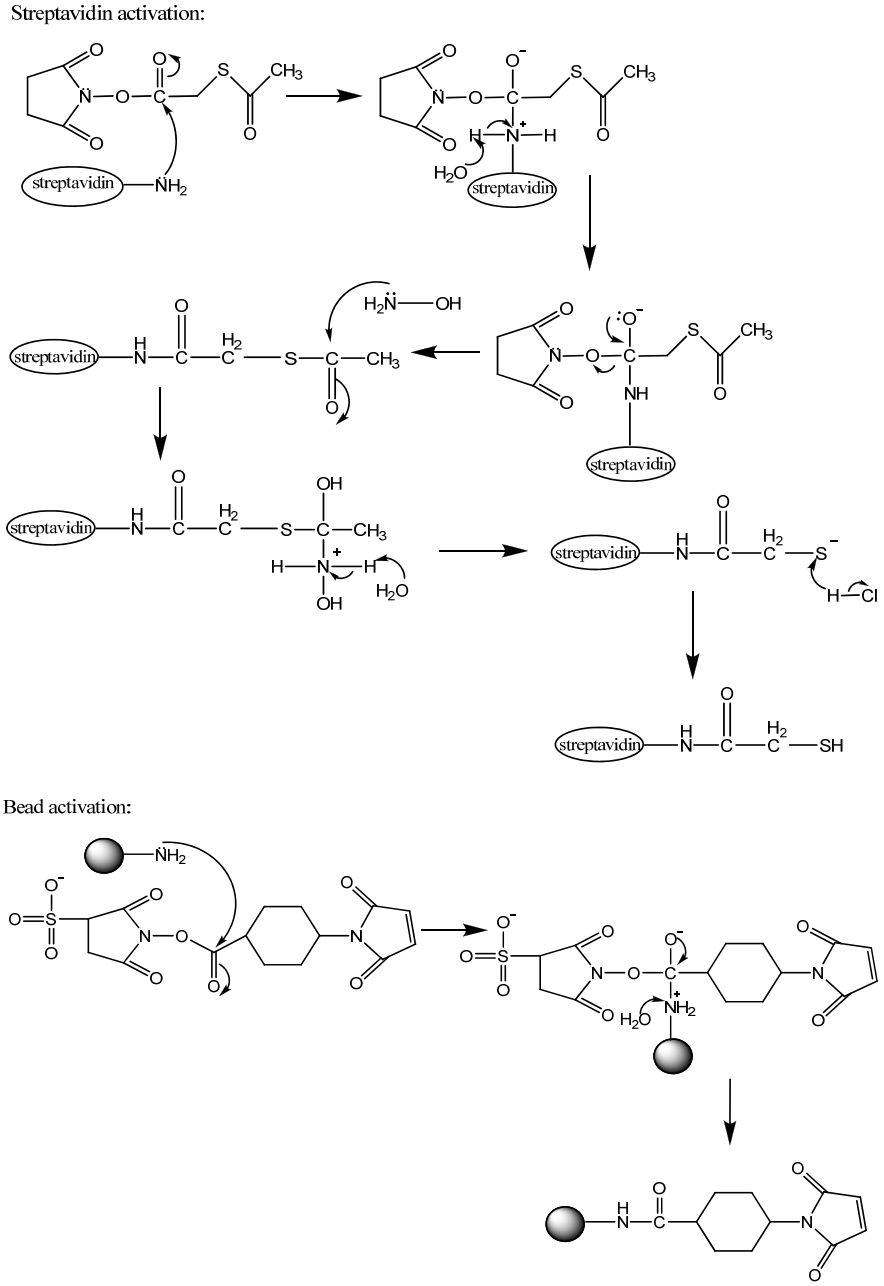

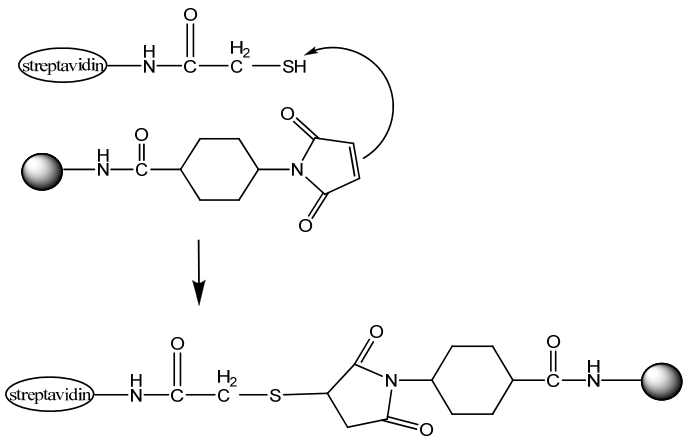

Fluorescent Nile Red aliphatic amine polystyrene beads from Invitrogen were used. The beads were part of a custom batch (Batch number 6-FLN-40.3, lot number 500983) with a mean diameter of 43 ± 6 nm and concentration 830 nM.

For the maleimide conjugation to the beads, 2 mg sulfo-SMCC (Pierce) was dissolved in 200 µL nanopure water, with mixing. 168 µL bead stock solution was added, and allowed to react for two hours at room temperature with rocking. Purification of the maleimide-activated beads from free sulfo-SMCC was performed using a Zeba desalt spin column (Pierce). For thiolation of streptavidin, 360 µL of 10mg/mL streptavidin (Thermo) was reacted with 18 µL of 6.5 mg/mL SATA for 30 minutes at room temperature with rocking. Deprotection of the thiol group now present on the streptavidin was achieved through use of a 0.5 M hydroxylamine hydrochloride (Thermo) solution in 0.1 M sodium phosphate pH 7.2 with 10 mM EDTA. 40 µL of the hydroxylamine solution was added to the thiolated streptavidin solution and allowed to react for two hours at room temperature.

For conjugation of the maleimide-activated beads and thiolated streptavidin, 210 µL of the bead-SMCC solution was added to all 420 µL of the deprotected streptavidin solution, and allowed to react at room temperature for 30 minutes with rocking. The resulting streptavidin-conjugated beads were purified from the free streptavidin using a

Zeba desalt spin column. The resulting solution was further purified from unconjugated beads using a G-25 sephadex column (GE Healthcare).

From UV-Vis analysis, it was determined that there are approximately 200 streptavidin molecules conjugated to each bead. Using biotin-4-fluorescein (Invitrogen), the biotin-binding capacity of the conjugated streptavidin was analyzed. Following a biotin-4-fluorescein assay protocol from Gruber, et al. [21], it was determined that each streptavidin conjugated to the beads had 2 biotin-binding sites available, equating to approximately 400 biotin-binding sites per bead.

At present, the beads are conjugated with biotin-active streptavidin. The beads were incubated with biotinylated polyarginine for five minutes at room temperature. The resulting polyarginine-conjugated beads were added to BS-C-1 cells in the presence and absence of pyrenebutyrate as in [20]. After a four minute incubation, the cells were washed and imaged to visualize bead uptake. It appears as though there was no uptake of the beads by the cells, even after an overnight incubation. Conjugation of the polyarginine to the beads will need to be confirmed through zeta potential measurements or use of a fluorescently tagged polyarginine sequence. In the event that conjugation is confirmed, smaller beads may need to be employed, as the size limit of the uptake mechanism may have been reached.

REFERENCES

[1] Lakowicz, J.R., *Principles of Fluorescence Spectroscopy,* 3rd Ed; Springer: New York, 2006.

[2] Day, R.N.; Schaufele, F., *Mol. Endocrinol*. **2005**, *19*, 1675-1686.

[3] Sambrook, J.; Russell, D.W., " Introducing Cloned Genes into Cultured Mammalian Cells," *Molecular Cloning A Laboratory Manual*, 3rd Ed, vol 3; Cold Spring Harbor: New York, 2001.

[4] Lakowicz, J.R., "Single –Molecule Detection," *Principles of Fluorescence Spectroscopy,* 3rd Ed; Springer: New York, 2006.

[5] Andrews, P.D.; Harper, I.S.; Swedlow, J.R.;*Traffic*, **2002**, *3*, 29-36
Litchman, J.; Conchello, J., *Nature Methods* **2005***, 2*, 910-919.

[6] Minsky, M, *Confocal Scanning Microscope* US Patent No 3013467,**1955**

[7] Piston, D., "Two-Photon Excitation Microscopy," *Fluorescence Imaging Microscopy and Spectroscopy*, XF Wang, B Herman, editors, John Wiley and Sons: New York, 1996.
Pawlicki, M.; Collins, H.A.; Denning, R.G.; Anderson, H.L., *Angew. Chem. Int. Ed*. **2009**, *48*, 3244-3266.

[8] Aubin, J.E., *J. Histochem. And Cytochem*. **1979**, *27*, 36-43.

[9] Hopps, H.E.; Bernheim, B.C.; Nisalak, A.; Tjio, J.H.; Smadel, J.E., *J. Immunol*. **1963**, *91*, 416-424.

[10] Axelrod, D., *Traffic* **2001**, *2*, 764-774.

[11] Walker, F.O., *Lancet* **2007**, *369*, 218-228.

[12] Macdonald, M.E.; Ambrose, M.P.; Duyao, R.H.; Myers, C.; Lin, L.; Srinidhi, G.; Barnes, S.A.; Taylor, M.; James, N.; Groot, H.; Macfarlane, B.; Jenkins, M.A.; Anderson, N.S.; Wexler, J.F.; Gusella, G.P.; Bates, S.; Baxendale, H.; Hummerich, S.; Kirby, M.; North, S.; Youngman, R.; Mott, G.; Zehetner, Z.; Sedlacek, A.; Poustka, A.M.; Frischauf, H.; Lehrach, A.J.; Buckler, D.; Church, L.; Doucettestamm, M.C.; Odonovan, L.; Ribaramirez, M.; Shah, V.P.; Stanton, S.A.; Strobel, K.M.; Draths, J.L.; Wales, P.; Dervan, D.E.; Housman, M.; Altherr, R.; Shiang, L.; Thompson, T.; Fielder, J.J.; Wasmuth, D.; Tagle, J.; Valdes, L.; Elmer, M.; Allard, L.; Castilla, M.; Swaroop, K.; Blanchard, F.S.; Collins, R.; Snell, T.; Holloway, K.; Gillespie, N.; Datson, D.; Shaw, and P.S. Harper, *Cell*, **1993**. *72*. 971-983

[13] Ammor, M.S., *J. Fluoresc*. **2007**, *17*, 455-459.

[14] Schapper, F.; Goncalves, J.T.; Oheim, M., *Eur. Biophys. J*. **2003**, *32*, 635-643. Gryczynski, I.; Gryczynski, Z.; Lakowicz, *J., Anal. Biochem*. **1997**, *247*, 69-76. Oheim, M.; Schapper, F., *J. Phys. D: Appl. Phys*., **2005**, *38*, R185-R197.

[15] Göppert-Mayer, M., *Ann. Phys.* **1931,** *9*, 273-295.

[16] Kaiser, W., Garrett, C.G.B., *Phys. Rev. Lett.* **1961**, *7*, 229-232.

[17] Denk, W.; Strickler, J.; Webb, W.W., *Science*, **1990**, *248*, 73-76

[18] Sauter, E.G., *Nonlinear Optics*, John Wiley and Sons: New York, 1996.

[19] Gossen, M.; Freundlieb, S.; Bender, G.; Muller, G.; Hillen, W.; Bujard, H., *Science*, **1995**, *268*, 1766-1769.

[20] Jablonski, A.E.; Humphries, W.H.; Payne, C.K., *J Phys. Chem. B*, **2009**, *113*, 405-408.

[21] Gruber, H.J.; Kada, G.; Marek, M.; Kaiser, K., *Biochim. Biophys. Acta* **1998**, *1381*, 203-212.